Predicting and identifying antimicrobial resistance in the marine environment using AI and machine learning algorithms.

FOUGH, F., JANJUA, G., ZHAO, Y. and DON, A.W.

2023

Predicting and Identifying Antimicrobial Resistance in the Marine Environment Using AI & Machine Learning Algorithms

Faranak Fough
School of Engineering
Robert Gordon University
Aberdeen, United Kingdom
f.fough@rgu.ac.uk

Dr Ghalib Janjua
School of Engineering
Robert Gordon University
Aberdeen, United Kingdom
g.janjua@rgu.ac.uk

Dr Yafan Zhao
School of Engineering
Robert Gordon University
Aberdeen, United Kingdom
y.zhao@rgu.ac.uk

Dr Aakash Welgamage Don
School of Pharmacy and Life Sciences
Robert Gordon University
Aberdeen, United Kingdom
a.welgamage-don@rgu.ac.uk

***Abstract*—Antimicrobial resistance (AMR) is an increasingly critical public health issue necessitating precise and efficient methodologies to achieve prompt results. The accurate and early detection of AMR is crucial, as its absence can pose life-threatening risks to diverse ecosystems, including the marine environment. The spread of AMR among microorganisms in the marine environment can have significant consequences, potentially impacting human life directly. This study focuses on evaluating the diameters of the disc diffusion zone and employs artificial intelligence and machine learning techniques such as image segmentation, data augmentation, and deep learning methods to enhance accuracy and predict microbial resistance.**

***Index Terms*—Artificial intelligence, Machine Learning methods, Inhibition zone measurement, Convolutional Neural Networks, Antimicrobial susceptibility test**

I. Introduction

Antimicrobial resistance (AMR) poses a significant threat to diverse ecosystem components, including human, animal and environmental [1]. In this study, our focus is specifically directed towards the microorganisms inhabiting marine environments. The development and transmission of AMR between microorganisms in marine environments can be attributed to various factors, such as horizontal gene transfer, gene mutation, and intrinsic resistance mechanisms [2]. It's worth noting that not all marine microorganisms exhibit resistance, and not all possess the capacity to develop resistance mechanisms. In this regard, human activities such as the discharge of treated wastewater, agricultural runoff, aquaculture practices, and the deposition of conventional and nuclear wastes have exacerbated this issue [3]. AMR has been detected in marine environments worldwide, including coastal waters and marine sediments. Numerous studies have raised concerns about the spread of AMR from marine microorganisms to other environments, with significant implications for public health [4].

Accurate analysis and measurement of AMR in marine microorganisms are essential for understanding the potential problems associated with environmental pollution and the spread of resistance. Therefore, the need for rapid and accurate tools to address these issues becomes critical. While various techniques exist for identifying and diagnosing bacterial susceptibility or resistance to antimicrobial agents in clinical settings, the most commonly used method in this field is the disc diffusion method [5]. Laboratories employ this method due to its simplicity, cost-effectiveness, and established interpretive criteria [5]. However, there are several challenges associated with its use that can impact result transparency, including delayed response time, labour-intensive procedures, etc [6]. With more details, The disc diffusion method has inherent challenges such as the slow turnaround time required for bacterial growth on agar plates and subjectivity in result interpretation, which relies on visual assessment with using a scope and ruler. This subjective process may introduce variability between different observers, affecting the accuracy of the results. But this method is still widely practised as a gold-standard tool for determining bacterial sensitivity in most clinical and health care areas [6]. In recent decades, artificial intelligence (AI) and machine learning (ML)techniques have come out as promising tools to address the limitations of the disc diffusion method [7]. Several research teams have utilised AI and ML algorithms to measure the zone of inhibition around antibiotic discs in images. This approach has been shown the potential to enhance the accuracy of disc diffusion zone diameter measurement. Employing these advanced computational approaches can greatly improve the efficiency and speed of assessing AMR in marine microorganisms, offering valuable insights for environmental management and public health considerations. The goal of this study is to replace the manual measurement, which involves using a scale to measure the zone of inhibition around the antibiotic disc. Instead, we used advanced algorithms and ML techniques to calculate the diameter. In this case, Algorithms that have been developed ought to work with any image from camera. Consequently, the development of an efficient automated technique that enables automatic image segmentation is required for the laboratory to use for diagnosis.In the context of AMR identification in marine microorganisms, we will have a particular focus on data augmentation, segmentation methods, and conventional neural network applications for detecting and measuring disc diffusion zone diameters with high accuracy. This will ulti-

mately enhance decision-making for researchers, reduce the risk of AMR through different human activities, and prevent the spread of AMR organisms.

II. BACKGROUND

The measurement of inhabitant zones in any disc diffusion test is challenging to standardize. This involves considering factors such as the measurement of zone diameter, inspection of the zone boundary, detection of colonies within the inhibitory zone, susceptibility of the organism to the antimicrobial agent, diffusion characteristics of the agent, and agent concentration [8]. Traditionally, a caliper or ruler is used by people to manually measure the diameter of the inhibitory zone. This manual process is labor-intensive, taking up to 72 hours, and prone to error [9]. Standardized interpretation is crucial. For example, for some combinations of organisms and agents, a sharp zone edge indicates the presence of a resistance mechanism, while for others, it may not. The lack of guidelines for interpretation can affect the result accuracy. To address this issue, scientific resources like the EUCAST disc diffusion test handbook and the EUCAST reading guide in Europe [10], which provide valuable interpretation guidelines to help standardize readings [11] [12] [13].To achieve accurate and faster results, an advanced level of expertise and tools for interpretation is required. Several automatic tools like the Oxoid aura image system [14], Antibiogramj [15], and image processing algorithms [9] [16] [17] [18], have improved accuracy and reduced running time. Ideally, to atomate measuring the inhibition zone effectually, addressing issues such as bacterial growth homogeneity, the overlap between inhibition zones, non-homogeneous growth, and the fractional action of an antibiotic is needed. In this study, We anticipate that AI, ML and deep learning methods will play a crucial role in measuring the zone diameter, and enabling rapid evaluation and interpretation of antimicrobial susceptibility testing (AST) using the disc diffusion method.

A. Segmentation

There are two distinct image segmentation approaches: Semantic segmentation classifies each pixel with a label and Instance segmentation classifies each pixel and differentiates each object instance [19]. Instance segmentation is the optimal choice for Automatic Inhibition Zone Diameter Measurement in Disc Diffusion Tests due to its precision in identifying individual inhibition zones, ensuring accurate measurements for antibiotic susceptibility evaluation. There are several common instance segmentation techniques are used for various segmentation challenges such as Modified edge detection, DeepLab, Mask R-CNN, UNet, Fully convolutions network(FCN), Hybrid approaches and etc. Notably, Mask R-CNN which is an instance segmentation method based on deep learning and U-Net which is Semantic segmentation demonstrate remarkable results in this area. In this paper, we aim to explore and compare different segmentation methods. We will leverage the power of convolutional neural networks (CNNs) for the automatic interpretation of AST. By employing these advanced techniques, we seek to enhance the accuracy, efficiency, and reliability of measuring the inhibition zone diameter in the disc diffusion method to classify the bacteria into three different classes.

1) U-Net Architecture: U-Net as a semantic segmentation technique is a CNN architecture commonly used for image segmentation tasks, is the most famous end-to-end FCN model, which is known for its ability to effectively segment objects in biomedical images [20]. Its distinctive U-shaped design comprises an encoder and decoder network connected through skip connections. The encoder part of the U-Net architecture uses successive convolutional and pooling layers to extract high-level features from the input image [20]. U-Net Segmentation algorithm could be simplified as follow: Consider the U-Net architecture with an encoder as E and a decoder as D. Let $input$ represent the input image, and let C denote the feature maps from the contracting path. The resulting segmentation map is given as S, and the concatenation operation is represented as $\oplus$:

$$S = D(E(input) \oplus C) \tag{1}$$

U-Net can learn to differentiate between foreground and background regions, enabling precise segmentation of objects of interest. The U-Net architecture has been successfully applied to various segmentation tasks, including disc diffusion test image segmentation [21]. In the U-Net method, after the image acquisition and pre-processing steps, the next crucial step is image enhancement. We utilize the stochastic gradient descent (SGD) optimization algorithm in Caffe, implemented using through the Solver and Net classes provided by the framework. Subsequently, diameter measurement is performed using a boundary-finding technique. Our input is a disc diffusion test image. Then the encoder will apply a series of convolutional and pooling layers to extract high-level features and reduce the spatial dimensions of the input image. Skip Connections will connect the output of each encoder layer to the corresponding decoder layer. Further, the decoder will upsample the feature maps using transposed convolutions and concatenate them with the corresponding feature maps from the encoder layers. The final segmentation map using a series of convolutional layers will be generated as our output. The below flowchart shows the sequential steps of the UNet architecture for semantic segmentation (Fig1). This architecture has demonstrated success in various segmentation tasks.

The U-Net algorithm combines the encoder and decoder paths through skip connections, allowing the network to capture both local and global context information while retaining fine-grained details from the input image. In this method, the energy function is computed by a pixel-wise soft-max over the final feature map combined with the cross entropy loss function. The soft-max is defined as the following equation:

$$p_k(x) = \frac{\exp(a_k(x))}{\sum_{k=1}^{K} \exp(a_k(x))}, \tag{2}$$

where $a_k(x)$ denotes the activation in feature channel k at the pixel position $x \in \Omega$ with $\Omega \subset \mathbb{Z}^2$. K is the number

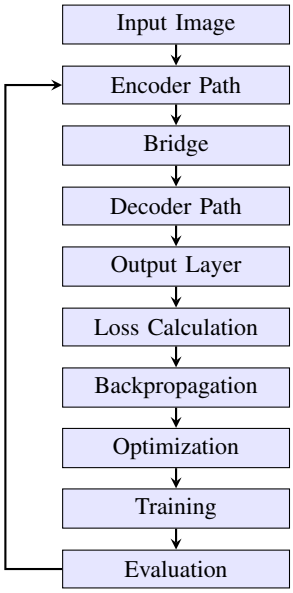

Fig. 1: Sequential Steps of the UNet Architecture for Semantic Segmentation

of classes, and $p_k(x)$ is the approximated maximum-function. That is, $p_k(x) \approx 1$ for the k that has the maximum activation $a_k(x)$, and $p_k(x) \approx 0$ for all other k. The cross-entropy then penalizes, at each position, the deviation of $p(x)(x)$ from 1 using:

$$E = \sum_{x \in \Omega} w(x) \log(p(x)(x)), \tag{3}$$

Where $\Omega \rightarrow \{1, ..., K\}$ is the true label of each pixel, and $w : \Omega \rightarrow \mathbb{R}$ is a weight map that we introduced to give some pixels more importance in the training. We pre-compute the weight map for each ground truth segmentation to compensate for the different frequency of pixels from a certain class in the training dataset and to force the network to learn the small separation borders that we introduce between touching cells.The separation border is computed using morphological operations. The weight map is then computed as:

$$w(x) = w_c(x) + w_0 \cdot \exp\left(-\frac{(d_1(x) + d_2(x))^2}{2\sigma^2}\right), \tag{4}$$

Where $w_c : \Omega \rightarrow \mathbb{R}$ is the weight map to balance the class frequencies, $d_1 : \Omega \rightarrow \mathbb{R}$ denotes the distance to the border of the nearest cell, and $d_2 : \Omega \rightarrow \mathbb{R}$ denotes the distance to the border of the second nearest cell. In our experiments, we set $w_0 = 10$ and $\sigma \approx 5$ pixels. Proper initialization of the weights is crucial in deep networks with multiple convolutional layers along with various network paths. Otherwise, certain regions of network could activate too much while other parts never do. The initial weights should be modified so the variance of each feature map in the network is about equal [21].

2) Mask R-CNN Architecture: Is more advanced and widely adopted framework for object detection and instance segmentation, following the 'detect-then-segment' strategy in the visual field [22] [23]. Which can be utilized for object

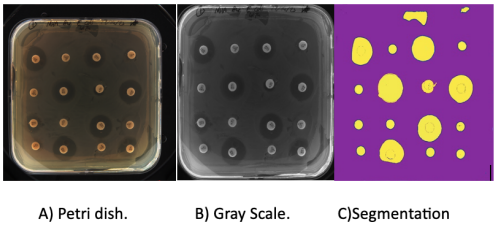

Fig. 2: Schematic diagram of U-Net methods

identification, accurately outlining the object's boundary, and detecting key points [27].The Mask R-CNN architecture builds upon the Faster R-CNN by adding the mask generation head. The backbone, RPN, RoIAlign, and bounding-box detection head are shared between Faster R-CNN and Mask R-CNN [22] [27]. The network architecture of Mask R-CNN can be illustrated As shown in the below flowchart (Fig3).

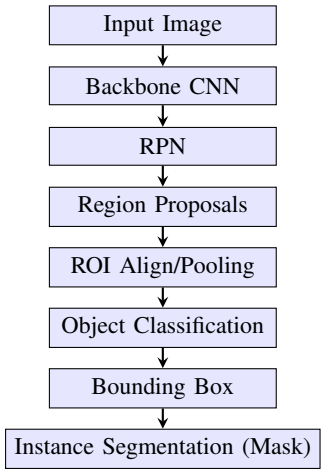

Fig. 3: Sequential Steps of the Mask R-CNN Algorithm for Object Detection and Instance Segmentation

The framework efficiently detects objects and simultaneously generates high-quality segmentation mask for each instance in an image. Mask R-CNN is known for its accurate instance segmentation capabilities. It can detect and segment multiple objects within an image, providing pixel-level masks for each instance. This makes it well-suited for tasks where precise localization and segmentation of individual objects are required [22]. Here is a simplified equation representing the mathematical formulation of the Mask R-CNN algorithm. Given the R-CNN object detection output as (C, B, M) where: C is class predictions. B is bounding box coordinates. M is the region of interest (RoI) feature maps. The mask prediction P is computed for each RoI using a mask head:

$$P = \text{Mask\_Head}(M)$$

In this study, the network will pass the image through a CNN to extract high-level features [22].To provide additional

insight, After finalizing the network architecture of Mask R-CNN, it was trained using Petri dish images and the corresponding annotation images. These annotation images were provided with an annotation tool to label the images. The labeled images were randomly split into a training set and a validation set to ensure the model's accuracy and stability. During training, minimizing the loss function improves its performance in both object detection (classification and bounding box regression) and instance segmentation (mask prediction) tasks [22] [23]. The CNN model provided optimal performance and results in this process. This trained model was then applied to predict and analyze new images.

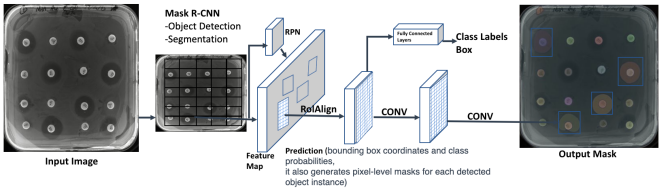

Fig. 4: Schematic Diagram of Mask R-CNN methods.

The total loss for Mask R-CNN is a combination of this three components [22]:

$$L_{\text{total}} = L_{\text{class}} + L_{\text{box}} + L_{\text{mask}} \tag{5}$$

Where Lclass + Lbox have been recognized in the same manner as in Faster R-CNN, their definition is as follows: we denote the predicted class probabilities as P_{class} and the ground-truth class labels as GT_{class}. The classification loss can be defined as:

$$L_{\text{class}} = -\sum_{i=1}^{N}\sum_{j=1}^{C} \text{GT}_{\text{class}}[i,j]\log(\text{P}_{\text{class}}[i,j]) \tag{6}$$

Where: N is the number of anchor locations (region proposals). C is the number of object classes.

$\text{GT}_{\text{class}}[i,j]$ is the ground-truth probability that anchor i corresponds to class j. $\text{P}_{\text{class}}[i,j]$ is the predicted probability assigned to anchor i for class j.

The bounding box regression loss is calculated using the smooth L1 loss function, which is less sensitive to outliers. Let's denote the ground-truth bounding box coordinates as GT_{box} and the predicted bounding box coordinates as P_{box}. The bounding box regression loss can be expressed as:

$$L_{\text{box}} = \sum_{i=1}^{N}\sum_{k=1}^{4} \text{smooth\_L1\_loss}(\text{GT}_{\text{box}}[i,k], \text{P}_{\text{box}}[i,k]) \tag{7}$$

Where: N is the number of anchor locations (region proposals). k represents the four coordinates of the bounding box: x, y, width, and height. $\text{GT}_{\text{box}}[i,k]$ is the ground-truth value of coordinate k for anchor i. $\text{P}_{\text{box}}[i,k]$ is the predicted value of coordinate k for anchor i.

The smooth L1 loss is defined as follows:

$$\text{smooth\_L1\_loss}(x) = \begin{cases} 0.5x^2 & \text{if } |x| < 1, \\ |x| - 0.5 & \text{otherwise.} \end{cases} \tag{8}$$

The bounding box regression loss is calculated using the smooth L1 loss function, which is less sensitive to outliers. Let's denote the ground-truth bounding box coordinates as GT_{box} and the predicted bounding box coordinates as P_{box}. The bounding box regression loss can be expressed as:

$$L_{\text{box}} = \sum_{i=1}^{N}\sum_{k=1}^{4} \text{smooth\_L1\_loss}(\text{GT}_{\text{box}}[i,k], \text{P}_{\text{box}}[i,k]) \tag{9}$$

Mask Prediction Loss (Lmask): The mask prediction loss measures the quality of the predicted instance masks. It is typically calculated using the binary cross-entropy loss. Let's denote the ground-truth binary masks as GT_{mask} and the predicted masks as P_{mask}. The mask prediction loss can be expressed as:

$$\begin{aligned} L_{\text{mask}} = &-\sum_{i=1}^{N}\sum_{p=1}^{M} \text{GT}_{\text{mask}}[i,p]\log(\text{P}_{\text{mask}}[i,p]) \\ &+ (1 - \text{GT}_{\text{mask}}[i,p])\log(1 - \text{P}_{\text{mask}}[i,p]) \end{aligned} \tag{10}$$

The model aims to minimise the total loss L_{total}.The performance of the trained Mask R-CNN model was quantitatively evaluated by mean average precision (mAP) metrics, to understand how accurate the model is in detecting and segmenting Petri dish in the validation set. A higher mAP indicates better performance in accurately localizing and segmenting objects in the validation. The mAP is obtained by taking the mean of all The Average Precision (AP) values across all classes. AP is calculated as follows:

$$mAP_i = \frac{Area(\text{A}_i \cap \text{B}_i)}{Area(\text{A}_i \cup \text{B}_i)} \tag{11}$$

where A is the model segmentation result and B is the corresponding Bacterial Contour[1] delineated by laboratory technicians using a microscope and ruler as ground truth. NT is the number of images. TP/FP determination is based on how you evaluate the overlap between the model's prediction and the ground truth annotation for bacterial growth diameter in Petri dish images and the measure of the true growth diameter.

$$\text{True Positive (TP)}_i = \begin{cases} 1, & \text{if } mAP_i \geq \text{mAP threshold} \\ 0, & \text{otherwise} \end{cases} \tag{12}$$

$$\text{False Positive (FP)}_i = \begin{cases} 1, & \text{if } mAP_i < \text{mAP threshold} \\ 0, & \text{otherwise} \end{cases} \tag{13}$$

$$\text{Precision} = \frac{\sum_{i=1}^{NT} \text{TP}_i}{\sum_{i=1}^{NT} \text{TP}_i + \sum_{i=1}^{NT} \text{FP}_i} \tag{14}$$

$$\text{Recall} = \frac{\sum_{i=1}^{NT} \text{TP}_i}{\text{Total number of true bacterial growth instances}} \tag{15}$$

$$\text{Average Precision (AP)} = \sum_{r} \Delta\text{recall}_r \cdot \max(\text{precision}_{\text{high}}(r)) \tag{16}$$

[1]The "Bacterial Contour" refers to the measurement of the zone or boundary of the bacterial colony or growth area present on the Petri dish image.

$$\text{mAP} = \frac{\sum_c \text{AP}_c}{\text{Number of classes}} \tag{17}$$

It is important to recognize that large databases of fully annotated medical images are required for the implementation of above approaches. However, in the medical domain, datasets are not readily accessible, and it is considered a time-consuming and labor-intensive procedure. There are several strategies and tailoring them to overcome this challenge, like the multi-instance learning methods (MIL) [28] or 3D Self-Supervised Methods for Medical Imaging [29].

B. Deep learning approaches

Over the past decade, deep CNN have consistently exhibited state-of-the-art performance in various biomedical image analysis applications and in many visual recognition tasks [24]. CNNs are typically employed in classification tasks, where the output to an image is a single or multiple-class label that represents the predicted category or categories for input image [25]. These networks have proven robust in handling challenges related to image quality, such as variations in lighting conditions, irregularities on agar plates, and the presence of debris or impurities. The development of deep learning algorithms has not only enabled accurate image detection but has also demonstrated superior capabilities in segmentation approaches [26]. CNNs are extensively utilized in image processing tasks, including image classification, object detection, and image segmentation, and have achieved remarkable results. CNNs have the ability to learn and extract complex patterns and features from diverse biomedical image datasets. Several studies [30] [31] [32] have employed CNNs for pathogen identification and detection in clinical diagnoses and pathogenesis studies, making them a suitable option for identifying and measuring the zones of inhibition in disc diffusion.Moreover, CNN models can accurately segment and measure the zones of inhibition without the need for human intervention. Convolutional layers within CNNs play a critical role by utilizing filters (kernels or feature detectors) to extract spatial and temporal features from input images [33]. This level of automation significantly improves the results.

III. Methodology

This study delves into the exploration and comparison of diverse segmentation methods, leveraging convolutions neural networks (CNNs) to automate the interpretation of AST. The overarching goal is to elevate the precision, efficiency, and dependability of measuring inhibition zone diameter, ultimately categorizing bacteria into three distinct classes.

Our study aims to harness deep learning algorithms for the analysis of microscopic images derived from disc diffusion tests. With a precise identification and measurement of antibiotic disc inhibition zones, we aspire to heighten decision-making processes and counteract the propagation of antibiotic-resistant microorganisms within marine ecosystems. The steps are done as follow: Step 1: Collect Microbial Samples, Microbial samples were obtained from marine ecosystems. Step 2: Prepare Agar Plates, the microbial samples were plated onto agar surfaces, and the plates were then incubated for 24 hours at 37°C. Step 3: Capture Images of Agar Plates, a ProtoCOL 3 Plus camera mounted on an all-in-one PC was used to capture images of the agar plates. Ensure onsistent lighting conditions and camera settings were maintained for all images. Step 4: Apply Segmentation Algorithms, the U-Net segmentation algorithm and Mask R-CNN segmentation algorithm were applied to the captured images. Step 5: Pair Segmented Images with Ground Truth, segmented images from both algorithms were matched with ground truth measurements of disc diffusion zone diameters. Step 6: Segmentation of Infected Cells: a segmentation method was employed to separate infected cells from the background in the images. Step 7: Automated Diameter Prediction, CNN was trained using a labeled dataset of disc diffusion images with known zone diameters. The CNN learned to predict zone diameters, automating measurements. Step 8: Inhibition Zone Identification, segmentation identified inhibition zones on the agar plates. Step 9: Classification of Zone Diameters: CNN predicted and classified zone diameters into resistance, intermediate, and susceptible categories. Step 10 : Model Evaluation, Sensitivity, specificity, accuracy, and other metrics were utilized to evaluate the deep learning model's performance. Comparative analyses with alternative methods were conducted to validate the proposed methodology's effectiveness.

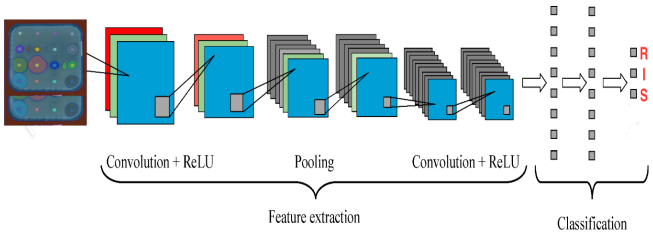

Fig. 5: CNN to predict in three classes Resistance(R), Intermediate(I), Susceptible(S)

Traditional methods often used as decision-making tools for clinicians, might not provide sufficient support for treatment choices due to concerns over operator-dependent discrepancies and the intricate nature of result interpretation. This automated measurement process anticipates the elimination of manual ruler-based measurements. The integration of segmentation and CNNs offers a solution for automating the measurement and evaluation process in disc diffusion testing, reducing manual effort, enhancing accuracy, and expediting the analysis of antimicrobial susceptibility test results.

IV. Conclusion and Future scope

This study introduces an advanced deep learning-based methodology for accurate measurement of disc diffusion zone diameters in AST. By utilizing the potential of deep learning algorithms and incorporating microbiological knowledge, our approach offers accurate identification and measurement of AMR. Our research aims to review the use of ML techniques

in segmenting and measuring inhibition zones in AST. Our methodology has the potential to improve AST by enhancing measurement accuracy and efficiency. By leveraging deep learning, it improves antimicrobial susceptibility analysis, aiding antibiotic selection and reducing resistance risks. Additionally, this work contributes to addressing environmental and public health concerns related to AMR. Precise measurements support informed decision-making, reduce antibiotic misuse, and promote prudent antimicrobial agent use. Adoption of our methodology can positively impact patient outcomes and global antimicrobial resistance efforts. While the proposed algorithm effectively identifies zones from images captured by any device, it currently faces a significant limitation due to extended execution time and improved solutions for zone identification tasks. Future works will concentrate on developing a new, optimized method that achieves substantial speed enhancements while maintaining desired accuracy and robustness levels. This pursuit entails leveraging advanced neural network architectures, with a focus on adopting deep learning architectures to minimize the semantic gap between encoder and decoder sub-networks, streamlining segmentation. Additionally, efforts will be directed toward making the method more applicable in real-world scenarios. Addressing this critical facet of image segmentation aims to make a substantial contribution to the field's advancement. We plan to conduct a user study for empirical and human evaluations of our models to assess their performance comprehensively.

REFERENCES

[1] Booton RD, Meeyai A, Alhusein N, Buller H, Feil E, Lambert H, Mongkolsuk S, Pitchforth E, Reyher KK, Sakcamduang W, Satayavivad J. One Health drivers of antibacterial resistance: quantifying the relative impacts of human, animal and environmental use and transmission. One Health. 2021 Jun 1;12:100220.

[2] Hejblum G, Jarlier V, Grosset J, Aurengo A. Automated interpretation of disk diffusion antibiotic susceptibility tests with the radial profile analysis algorithm. Journal of Clinical Microbiology. 1993 Sep;31(9):2396-2401. DOI: 10.1128/jcm.31.9.2396-2401.1993. PMID: 8408562; PMCID: PMC265768

[3] Bauer AW, Kirby WM, Sherris JC, Turck M. Antibiotic susceptibility testing by a standardized single disk method. Am J Clin Pathol. 1966 Apr;45(4):493-6. PMID: 5325707.

[4] Leonard AF, Morris D, Schmitt H, Gaze WH. Natural recreational waters and the risk that exposure to antibiotic-resistant bacteria poses to human health. Current Opinion in Microbiology. 2022 Feb 1;65:40-6.

[5] Reller LB, Weinstein M, Jorgensen JH, Ferraro MJ. Antimicrobial susceptibility testing: a review of general principles and contemporary practices. Clinical infectious diseases. 2009 Dec 1;49(11):1749-55.

[6] Salam MA, Al-Amin MY, Pawar JS, Akhter N, Lucy IB. Conventional methods and future trends in antimicrobial susceptibility testing. Saudi journal of biological sciences. 2023 Feb 10:103582.

[7] Testing, European Committee on Antimicrobial Susceptibility. "Breakpoint tables for interpretation of MICs and zone diameters." (2016).

[8] Priya, B.K., Reddy, D.A., Rani, A.D., Kalahasthi, N., Soliman, W.G. and Reddy, D.R.K., 2021. Automatic Inhibition Zone Diameter Measurement for Disc Diffusion Test Using Image Segmentation. IETE Journal of Research, pp.1-18.

[9] Pascucci, M., Royer, G., Adamek, J., Asmar, M.A., Aristizabal, D., Blanche, L., Bezzarga, A., Boniface-Chang, G., Brunner, A., Curel, C. and Dulac-Arnold, G., 2021. AI-based mobile application to fight antibiotic resistance. Nature communications, 12(1), p.1173.

[10] European Committee on Antimicrobial Susceptibility Testing. EUCAST disk diffusion test manual. Version 6.0. 2017.

[11] EUCAST, "The European Committee on Antimicrobial Susceptibility Testing - EUCAST." [Online]. Available: https://www.eucast.org. [Accessed: 19/Jun/2023].

[12] European Committee on Antimicrobial Susceptibility Testing, 2019. Reading Guide–EUCAST Disk Diffusion Method for Antimicrobial Susceptibility Testing. Version, 8, pp.1-30.

[13] Zone Diameters of antimicrobial agents according to CLSI guidlines.[Online]. Available:https://www.microrao.com/micronotes/pg/kirby_bauer.pdf.(2011).

[14] Lestari, E.S., Severin, J.A., Filius, P.M.G., Kuntaman, K., Duerink, D.O., Hadi, U., Wahjono, H. and Verbrugh, H.A., 2008. Comparison of the accuracy of disk diffusion zone diameters obtained by manual zone measurements to that by automated zone measurements to determine antimicrobial susceptibility. Journal of microbiological methods, 75(2).

[15] Alonso, C A et al. "Antibiogramj: A tool for analysing images from disk diffusion tests." Computer methods and programs in Biomedicine vol. 143 (2017): 159-169. doi:10.1016/j.cmpb.2017.03.010.

[16] Gavoille A, Bardy B, Andremont A. Measurement of inhibition zone diameter in disk susceptibility tests by computerized image analysis. Computers in biology and medicine. 1994 May 1;24(3):179-88.

[17] Khan, Z.A., Siddiqui, M.F. and Park, S., 2019. Current and emerging methods of antibiotic susceptibility testing. Diagnostics, 9(2), p.49.

[18] Costa, L.F., da Silva, E.S., Noronha, V.T., Vaz-Moreira, I., Nunes, O.C. and de Andrade, M.M., 2015. Development of an automatic identification algorithm for antibiogram analysis. Computers in biology and medicine, 67, pp.104-115.

[19] Chen LC, Hermans A, Papandreou G, Schroff F, Wang P, Adam H. Masklab: Instance segmentation by refining object detection with semantic and direction features. In Proceedings of the IEEE Conference on Computer Vision and Pattern Recognition 2018 (pp. 4013-4022).

[20] Du G, Cao X, Liang J, Zhan Y. Medical image segmentation based on u-net: A review. Journal of Imaging Science & Technology. 2020 Mar.

[21] Ronneberger O, Fischer P, Brox T. U-net: Convolutional networks for biomedical image segmentation. InMedical Image Computing and Computer-Assisted Intervention–MICCAI 2015: 18th International Conference, Munich, Germany, October 5-9, 2015, Proceedings, Part III 18 2015 (pp. 234-241). Springer International Publishing.

[22] He K, Gkioxari G, Girshick R. Mask r-cnn. In Proceedings of the IEEE International Conference on computer vision 2017 (pp.2961-2969).

[23] Wang X, Kong T, Shen C, Jiang Y, Li L. Solo: Segmenting objects by locations. InComputer Vision–ECCV 2020: 16th European Conference, Glasgow, UK, August 23–28, 2020, Proceedings, Part XVIII 16 2020 (pp. 649-665). Springer International Publishing.

[24] Cao C, Liu F, Tan H, Song D, Shu W, Li W, Zhou Y, Bo X, Xie Z. Deep learning and its applications in biomedicine. Genomics, proteomics & bioinformatics. 2018 Feb 1;16(1):17-32.

[25] Tiwari V, Joshi RC, Dutta MK. Dense convolutional neural networks based multiclass plant disease detection and classification using leaf images. Ecological Informatics. 2021 Jul 1;63:101289.

[26] Zhang Y, Jiang H, Ye T, Juhas M. Deep learning for imaging and detection of microorganisms. Trends in Microbiology. 2021 Jul 1;29(7):569.

[27] Shu JH, Nian FD, Yu MH, Li X. An improved mask R-CNN model for multiorgan segmentation. Mathematical Problems in Engineering. 2020 Jul 24;2020:1-1.

[28] Schwab E, Gooßen A, Deshpande H, Saalbach A. Localization of critical findings in chest X-ray without local annotations using multi-instance learning. In2020 IEEE 17th International Symposium on Biomedical Imaging (ISBI) 2020 Apr 3 (pp. 1879-1882).

[29] Taleb A, Loetzsch W, Danz N, Severin J, Gaertner T, Bergner B, Lippert C. 3d self-supervised methods for medical imaging. Advances in neural information processing systems. 2020;33:18158-72.

[30] Cai L, Gao J, Zhao D. A review of the application of deep learning in medical image classification and segmentation. Annals of translational medicine. 2020 Jun;8(11).

[31] Das DK, Chakraborty C. Computational microscopic imaging for malaria parasite detection: a systematic review. Journal of microscopy. 2015 Oct;260(1):1-9

[32] Goldsmith CS, Miller SE. Modern uses of electron microscopy for detection of viruses. Clinical microbiology reviews. 2009 Oct;22(4):552.

[33] Yang, R. and Yu, Y., 2021. Artificial convolutional neural network in object detection and semantic segmentation for medical imaging analysis. Frontiers in oncology, 11, p.638182.